Journal of Solid State Chemistry 183 (2010) 465–470

Contents lists available at ScienceDirect

Journal of Solid State Chemistry

journal homepage: www.elsevier.com/locate/jssc

Crystal growth, structure and magnetic properties of the double perovskites Ln_2MgIrO_6 (Ln=Pr, Nd, Sm–Gd)

Samuel J. Mugavero III, Adam H. Fox, Mark D. Smith, Hans-Conrad zur Loye *

Department of Chemistry and Biochemistry, University of South Carolina, Columbia, South Carolina 29208, USA

ARTICLE INFO

Article history:
Received 29 July 2009
Received in revised form
21 October 2009
Accepted 21 November 2009
Available online 11 December 2009

Keywords:
Crystal growth
Double perovskite
Hydroxide flux
Crystal structure
Magnetic properties
Pr_2MgIrO_6
Nd_2MgIrO_6
Sm_2MgIrO_6
Eu_2MgIrO_6
Gd_2MgIrO_6

ABSTRACT

Single crystals of double-perovskite type lanthanide magnesium iridium oxides, Ln_2MgIrO_6 (Ln=Pr, Nd, Sm–Gd) have been grown in a molten potassium hydroxide flux. The compounds crystallize in a distorted 1:1 rock salt lattice, space group $P2_1/n$, consisting of corner shared MO_6 (M=Mg^{2+} and Ir^{4+}) octahedra, where the rare earth cations occupy the eight-fold coordination sites formed by the corner shared octahedra. Pr_2MgIrO_6, Nd_2MgIrO_6, Sm_2MgIrO_6, and Eu_2MgIrO_6 order antiferromagnetically around 10–15 K.

© 2009 Elsevier Inc. All rights reserved.

1. Introduction

Perovskites are one of the most widely studied families of oxides owing greatly to their synthetic variability, compositional flexibility and intriguing properties. The discovery of new perovskites can be carefully postulated based on radius ratio rules. There is a vast library of known compositions with the general formula ABO_3, where A is large electropositive atom and B is a smaller atom [1], which is undoubtedly directly related to the ease with which cationic substitutions can be achieved in this family. The number of possible compositions can be further expanded when one allows for consideration of the compounds that adopt the double perovskite structure, with general formula $A_2BB'O_6$. Similarly, if one allows for cation substitutions with two different metals on the A-site such as in compounds with the formula $AA'BB'O_6$ as exemplified by $BaLaCoIrO_6$ [2], B-site substitutions of two metals of similar size and charge as in Nd_2BOsO_6, (B=Na, Li) [3,4], or B' site substitutions of two metals of similar size and available charge as demonstrated by $La_2NaB'O_6$ (M=Ru, Ir) [5–7], it becomes very apparent that not only are there already a large number of compositions in existence, but also that many new compositions can be prepared. In fact, taking into consideration radius ratio rules, the solid state chemist can confidently postulate the existence of an abundance of potential compositions in the ABO_3 [8] family and a seemingly unquantifiable number of compositions in the more complex double perovskite family. The ability to postulate compositions drives the synthetic chemist to pursue the discovery of new materials and the investigation of their physical properties.

The preparation of specific double perovskite compositions is commonly approached via the traditional solid-state synthetic method which, of course, requires a target composition. For example, the powder preparation, structural characterization, and magnetic properties of the double perovskite, La_2MgIrO_6 were previously reported [2,9]. Interestingly, until now, there have not been any reports on the incorporation of lanthanide metals with ionic radii smaller than lanthanum into the Ln_2MgIrO_6 type double perovskites. Our initial attempts to prepare the title compounds by traditional solid state techniques yielded unfavorable results where the desired phases formed with impurity phases, such as the defect fluorites with the general formula Ln_3IrO_7 (Ln=Pr, Nd, Sm, Eu) [10] or with an unreacted starting reagent, such as magnesium oxide, in the product. Where traditional solid state synthetic techniques encounter limits, another method, materials discovery by crystal growth using hydroxide fluxes [11], has been established as an excellent

* Corresponding author.
E-mail address: zurloye@mail.chem.sc.edu (H.-C. zur Loye).

0022-4596/$ - see front matter © 2009 Elsevier Inc. All rights reserved.
doi:10.1016/j.jssc.2009.11.025

approach for preparing compounds with targeted compositions and structure types that can be rationalized by radius ratio rules and new compounds with unique compositions and structures [12,13].

Our attempt to circumvent some of the limitations of traditional solid-state synthetic techniques using hydroxide flux reactions has resulted in the preparation of high quality single crystals of the title compounds. The crystal growth, structural characterization, and magnetic properties of Pr_2MgIrO_6, Nd_2MgIrO_6, Sm_2MgIrO_6, Eu_2MgIrO_6, and Gd_2MgIrO_6 are reported herein.

2. Experimental

2.1. Crystal growth

For all compounds, the lanthanide sesquioxides, Ln_2O_3 (Nd, Sm, Eu, Gd), (Alfa Aesar, 99.99%) were fired at 1000 °C for 12 h prior to the reactions. Pr_6O_{11} (Alfa Aesar, 99.9%) was converted to Pr_2O_3 by heating Pr_6O_{11} at 1000 °C for 24 h under a reducing 5% H_2 atmosphere. KOH (Fisher Scientific, A.C.S Reagent Grade, 99.9%), iridium powder (Engelhard, 99.99%) and MgO (Alfa Aesar, 99.998%) were used as received. Single crystals of Ln_2MgIrO_6 were grown from a high temperature melt of potassium hydroxide. Ln_2O_3 (Pr, Nd, Sm, Eu, Gd) (0.5 mmol), MgO (1 mmol), Ir (0.5 mmol), and KOH (4 g) were loaded into sealed silver tubes and heated in a box furnace to a temperature of 700 °C at 10 °C/min, held for 24 h at 700 °C, slow cooled to 600 °C at 0.2 °C/min and then allowed to cool to room temperature by turning off the furnace. The black crystals were removed from the flux matrix by dissolving the flux in water aided by sonication. The crystals were finally extracted by vacuum filtration.

2.2. Scanning electron microscopy

Single crystals of Ln_2MgIrO_6 (Ln=Pr, Nd, Sm–Gd) were analyzed by scanning electron microscopy using an FEI Quanta SEM instrument utilized in the low vacuum mode. Energy dispersive spectroscopy verified the presence of Mg, Ir, O and the respective lanthanide element, and within the detection limits of the instrument, confirmed the absence of extraneous elements, such as potassium and silver. A scanning electron micrograph of a single crystal of Sm_2MgIrO_6 is shown in Fig. 1.

2.3. Structural determination

For the structure determination of Ln_2MgIrO_6 (Ln=Pr, Nd, Sm, Eu, Gd), X-ray diffraction intensity data were measured at 294(2) K using a Bruker SMART APEX diffractometer (Mo$K\alpha$ radiation, λ=0.71073 Å) [14]. Each data collection covered a minimum of 99.1% of reciprocal space to $2\theta_{max}$=75°, with a minimum reflection redundancy to $2\theta_{max}$ of 4.3. The raw area detector data frames were processed with SAINT+ [14]. An absorption correction based on the redundancy of equivalent reflections was applied to the data with SADABS [14]. Reported unit cell parameters were determined by least-squares refinement of all reflections from the data sets with $I > 10\sigma(I)$. Full-matrix least-squares refinement against F^2 and difference Fourier calculations and were performed with SHELXTL [14].

The compounds adopt the monoclinic double perovskite structure type, in the space group $P2_1/n$. Refinement of this structural model converged rapidly. The β angle is near 90° in all cases; however, the pattern of systematic absences in the intensity data was not consistent with any orthorhombic space group. The asymmetric unit in $P2_1/n$ consists of three metal and three oxygen atom positions: Ln1 is on a general position (Wyckoff symbol 4*e*), Mg1 is on an inversion center (Wyckoff symbol 2*a*), Ir1 is on an inversion center (Wyckoff symbol 2*b*) and oxygen atoms O1–O3 are on general positions. Atoms were generally refined with anisotropic displacement parameters. The exception to this is the magnesium atom, which could be refined anisotropically only for Ln=Nd and Gd. Mg1 was refined isotropically for Ln=Pr, Sm and Eu. The reason for this is not clear, but likely due to the combined effects of moderate crystallinity and twinning in the specific systems. Trial refinements of site occupancy parameters showed no significant deviations from unity occupancy for the lanthanide or iridium atoms in any case. Because of the metrical similarity of the lattice to orthorhombic, all compounds except Ln=Gd were twinned to emulate orthorhombic symmetry. These refinements included the twin law [100/0-10/00-1] (two-fold rotation around [100]). The refined major twin fractions are Pr, 0.515(3); Nd, 0.796(3); Sm, 0.540(3); Eu, 0.656(3). Trial twin refinement of the Ln=Gd dataset gave a major twin fraction within experimental error of 1.0, with no improvement in *R*-values. The largest residual difference map peak/hole for the compounds are Pr: $+3.22/-2.82\,e^-/Å^3$, located 0.71 Å from Ir1/0.39 Å from Pr1; Nd: $+4.09/-3.54\,e^-/Å^3$, located 0.58 Å from Ir1/0.56 Å from Nd1; Sm: $+3.82/-2.68\,e^-/Å^3$, located 0.69 Å from Ir1/0.41 Å from Sm1; Eu: $+2.71/-2.69\,e^-/Å^3$, located 0.74 Å from Ir1/1.10 Å from Eu1; Gd: $+4.01/-2.80\,e^-/Å^3$, located 0.63 Å/0.57 Å from Ir1, respectively. Relevant crystallographic data for the five materials are presented in Table 1, atomic positions are given in Table 2, and selected interatomic distances and bond angles are listed in Table 3.

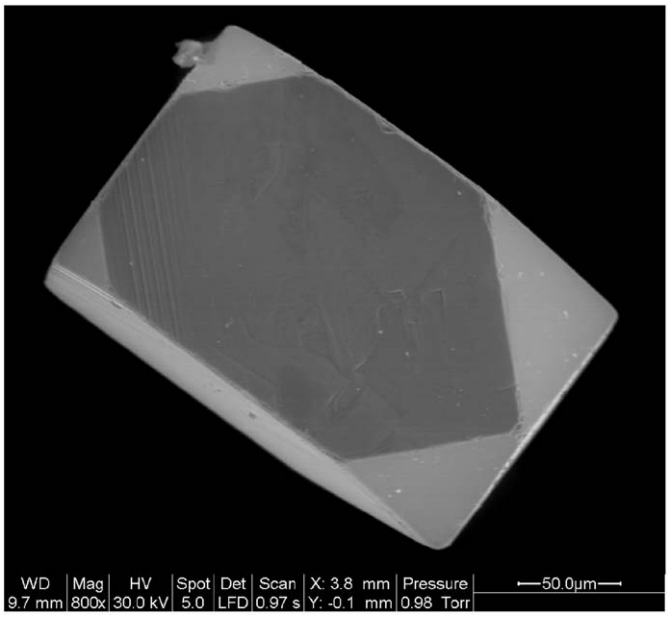

Fig. 1. An environmental scanning electron microscope image of a Sm_2MgIrO_6 single crystal.

2.4. Magnetic measurements

The magnetic susceptibility measurements of loose single crystals of Pr_2MgIrO_6, Nd_2MgIrO_6, Sm_2MgIrO_6, Eu_2MgIrO_6, and Gd_2MgIrO_6 were performed using a Quantum Design MPMS XL SQUID magnetometer. The samples were measured under both zero field cooled (ZFC) and field cooled (FC) conditions in applied fields of 1 and 10 kG over the temperature range of $5\,K \le T \le 300\,K$. The samples were contained in gel capsules suspended in a plastic straw for immersion into the SQUID.

Table 1
Crystal data and structural refinement for Pr_2MgIrO_6, Nd_2MgIrO_6, Sm_2MgIrO_6, Eu_2MgIrO_6, and Gd_2MgIrO_6.

Empirical formula	Pr_2MgIrO_6	Nd_2MgIrO_6	Sm_2MgIrO_6	Eu_2MgIrO_6	Gd_2MgIrO_6
Formula weight ($g\,mol^{-1}$)	594.33	600.99	613.21	616.43	627.01
Space group	$P2_1/n$	$P2_1/n$	$P2_1/n$	$P2_1/n$	$P2_1/n$
Unit cell dimensions					
a (Å)	5.5017(2)	5.4787(2)	5.4197(1)	5.3919(2)	5.3654(4)
b (Å)	5.6576(2)	5.6517(2)	5.6715(1)	5.6797(2)	5.6870(5)
c (Å)	7.8306(3)	7.8125(3)	7.7498(2)	7.7258(3)	7.7013(6)
β (deg)	90.006(2)	90.021(1)	90.013(1)	90.059(1)	90.193(3)
V (Å^3)	243.739(15)	241.906(15)	238.212(9)	236.598(15)	234.99(3)
Z	2	2	2	2	2
Density (calculated) ($g\,cm^{-3}$)	8.098	8.251	8.549	8.653	8.861
Absorption coefficient (mm^{-1})	46.985	48.664	52.273	54.320	56.224
F(000)	510	514	522	526	530
Crystal size (mm)	$0.04\times0.03\times0.02$	$0.05\times0.04\times0.02$	$0.06\times0.05\times0.04$	$0.04\times0.03\times0.02$	$0.06\times0.04\times0.03$
θ_{max} (deg)	37.80	37.83	37.80	37.78	37.93
Reflections collected	6867	7119	7032	5931	6637
Independent reflections	1322 (R_{int}=0.0418)	1305 (R_{int}=0.0348)	1280 (R_{int}=0.0310)	1263 (R_{int}=0.0458)	1260 (R_{int}=0.0355)
Goodness-of-fit on F^2	1.061	1.137	1.165	1.076	1.137
R indices (all data)	$R1$=0.0364, w$R2$=0.0630	$R1$=0.0324, w$R2$=0.0599	$R1$=0.0270, w$R2$=0.0595	$R1$=0.0423, w$R2$=0.0576	$R1$=0.0314 w$R2$=0.0627
Largest diff. peak/hole (e^- Å^{-3})	3.222/−2.815	4.085/−3.543	3.822/−2.677	2.710/−2.692	4.005/−2.803

Table 2
Atomic coordinates and equivalent isotropic displacement parameters for Pr_2MgIrO_6, Nd_2MgIrO_6, Sm_2MgIrO_6, Eu_2MgIrO_6, and Gd_2MgIrO_6, respectively.

	x	y	z	U_{eq}
Pr_2MgIrO_6				
Pr	0.4878(1)	0.0528(1)	0.2504(1)	0.010(1)
Mg	0	0	0	0.008(1)
Ir	1/2	1/2	0	0.008(1)
O1	0.2039(13)	0.2987(12)	0.0471(8)	0.011(1)
O2	0.5899(10)	0.4734(9)	0.2470(8)	0.012(1)
O3	0.3015(14)	0.7925(12)	0.0476(8)	0.012(1)
Nd_2MgIrO_6				
Nd	0.4869(1)	0.0543(1)	0.2504(1)	0.011(1)
Mg	0	0	0	0.008(1)
Ir	1/2	1/2	0	0.007(1)
O1	0.2046(9)	0.3000(9)	0.0471(7)	0.011(1)
O2	0.5927(9)	0.4735(8)	0.2467(7)	0.011(1)
O3	0.3044(9)	0.7933(9)	0.0479(7)	0.012(1)
Sm_2MgIrO_6				
Sm	0.4841(1)	0.0622(1)	0.2507(1)	0.010(1)
Mg	0	0	0	0.007(1)
Ir	1/2	1/2	0	0.007(1)
O1	0.1990(12)	0.3056(11)	0.0520(8)	0.011(1)
O2	0.6006(8)	0.4680(8)	0.2466(8)	0.011(1)
O3	0.3109(12)	0.7953(11)	0.0519(7)	0.010(1)
Eu_2MgIrO_6				
Eu	0.4826(1)	0.0652(1)	0.2509(1)	0.010(1)
Mg	0	0	0	0.007(1)
Ir	1/2	1/2	0	0.007(1)
O1	0.1975(12)	0.3041(13)	0.0527(9)	0.013(1)
O2	0.6055(10)	0.4638(10)	0.2467(8)	0.010(1)
O3	0.3140(13)	0.7986(12)	0.0539(8)	0.012(1)
Gd_2MgIrO_6				
Gd	0.4817(1)	0.0680(1)	0.2506(1)	0.010(1)
Mg	0	0	0	0.009(1)
Ir	1/2	1/2	0	0.008(1)
O1	0.1943(6)	0.3062(7)	0.0540(5)	0.011(1)
O2	0.6088(7)	0.4620(6)	0.2478(5)	0.010(1)
O3	0.3122(6)	0.7986(7)	0.0562(5)	0.011(1)

U_{eq} is defined as one third of the trace of the orthogonalized U_{ij} tensor.

The small diamagnetic contribution of the gelatin capsule containing the sample had negligible contribution to the overall magnetization, which was dominated by the sample.

Table 3
Selected interatomic distances (Å), bond angles (deg) and tolerance factors for Pr_2MgIrO_6, Nd_2MgIrO_6, Sm_2MgIrO_6, Eu_2MgIrO_6, and Gd_2MgIrO_6.

	Pr_2MgIrO_6	Nd_2MgIrO_6	Sm_2MgIrO_6	Eu_2MgIrO_6	Gd_2MgIrO_6
Ln–O(1)	2.386(7)	2.381(5)	2.333(6)	2.334(7)	2.320(4)
Ln–O(1)	2.629(8)	2.616(5)	2.581(7)	2.558(7)	2.326(4)
Ln–O(1)	2.741(7)	2.733(5)	2.715(6)	2.706(7)	2.548(4)
Ln–O(2)	2.367(6)	2.348(5)	2.313(5)	2.294(5)	2.278(4)
Ln–O(2)	2.445(5)	2.439(4)	2.386(5)	2.359(6)	2.342(4)
Ln–O(3)	2.396(8)	2.383(5)	2.355(6)	2.331(7)	2.326(4)
Ln–O(3)	2.622(7)	2.618(5)	2.578(6)	2.568(7)	2.537(4)
Ln–O(3)	2.749(7)	2.736(5)	2.718(6)	2.711(7)	2.720(4)
Mg–O(1) (×2)	2.062(6)	2.065(5)	2.081(6)	2.045(9)	2.069(7)
Mg–O(2) (×2)	2.048(6)	2.049(5)	2.046(6)	2.135(9)	2.049(6)
Mg–O(3) (×2)	2.066(7)	2.070(5)	2.085(6)	2.147(10)	2.085(6)
Ir–O(1) (×2)	2.002(6)	2.008(4)	2.010(6)	2.016(6)	2.020(3)
Ir–O(2) (×2)	2.018(6)	1.999(5)	1.995(6)	1.999(6)	2.006(4)
Ir–O(3) (×2)	2.022(6)	2.009(5)	2.004(6)	2.014(7)	2.022(4)
Ir–O(1)–Mg	150.2(4)	150.1(3)	147.0(3)	146.8(5)	146.8(4)
Ir–O(2)–Mg	150.4(3)	149.6(3)	146.9(3)	146.0(5)	145.2(3)
Ir–O(3)–Mg	150.2(4)	149.5(3)	147.1(3)	145.6(5)	145.6(4)
t	0.9101	0.8987	0.8929	0.8881	0.8850

3. Results and discussion

3.1. Synthetic considerations

Previously, we investigated the $Ln_2M^+Ir^{5+}O_6$ ((*Ln*=La, Pr, Nd–Gd; M^+=Li, Na) [5,7,15] system of double perovskites and established reactions parameters that were used to determine the reaction conditions for the title compounds. To prepare the lithium containing compounds with general formula, Ln_2LiIrO_6 (*Ln*=La, Pr, Nd, Sm, Eu), a two component LiOH/KOH flux (selected because it yielded higher quality single crystals than LiOH by itself) was used because K^+ has a six-coordinate ionic radius too large (1.38 Å) [16] to be incorporated into the octahedral site of the double perovskite structure and thus would not provide competition with the Li^+ cation (CN-6=0.76 Å) [16] for incorporation into the desired structure. Similarly, to prepare the Ln_2NaIrO_6 (*Ln*=La, Pr, Nd) double perovskites, sodium hydroxide was used

because the Na^+ cation was to be incorporated into the desired phases. Additionally, the crystal growth of $La_{2.5}K_{1.5}IrO_7$ [17] from a potassium hydroxide flux and $La_9RbIr_4O_{24}$ [18] from a rubidium hydroxide further established the exceptional synthetic utility of alkali metal hydroxide fluxes for crystal growth of complex lanthanide containing iridium oxides. To prepare the desired title compounds several hydroxide fluxes were tried, including $Mg(OH)_2$, KOH, RbOH, CsOH and the two component fluxes $Mg(OH)_2$/KOH, $Mg(OH)_2$/RbOH, and $Mg(OH)_2$/CsOH. Ultimately, a potassium hydroxide flux produced the desired phases using magnesium oxide as the source of Mg^{2+} for incorporation into the Ln_2MgIrO_6 composition. As in the case of the Ln_2LiIrO_6 series, the large ionic radius of K^+ did not provide competition for the Mg^{2+} (CN-6=0.72 Å) cation [16].

3.2. Crystal structure

The crystal structure of Nd_2MgIrO_6 is shown in Fig. 2 and is representative of the series of Ln_2MgIrO_6 (*Ln*=Pr, Nd, Sm–Gd) compounds that crystallize in the space group $P2_1/n$ with the monoclinic-distorted double perovskite structure [1]. The $P2_1/n$ space group allows for a 1:1 ordered arrangement of the B and B′ cations in a rock-salt type lattice and the tilting of the BO_6 and $B'O_6$ octahedra to accommodate the small size of the A cation. The Glazer tilt system assigned to the $P2_1/n$ space group is #10, *a*-*a*-*b*+ [19–21]. In the title compounds, the Mg^{2+} and Ir^{4+} cations lie on the two crystallographically independent octahedral sites, while the Ln^{3+} cations occupy the *A* site in an eight-fold coordination environment. The structural distortion in the title compounds occurs because the MO_6 octahedra must tilt to maintain their corner-sharing connectivity while creating favorable Ln–O distances. This type of distortion is commonly observed in perovskites containing small A-cations. The A–O bond lengths are limited to a narrow range and, therefore, the only means for the structure to accommodate smaller A-cations is by distorting the Mg–O–Ir bond angle. From a geometric standpoint, a smaller A-cation results in a more distorted *M*–O–*M* angle (away from the ideal value of 180°), and consequently the β angle of a monoclinic unit cell can be considered a measure of the structural distortion. In the case of the title compounds, as expected, the Mg–O–Ir angles decrease with decreasing size of the lanthanide cation while, concomitantly, the β angle increases except in the case of Sm_2MgIrO_6 (see Table 3).

While the double perovskite structure is stable for the title compounds, it appears unable to accommodate compositions with Ln^{3+} cations with an eight-coordinate ionic radius smaller than that of Gd^{3+}. Efforts to synthesize these analogs were unsuccessful and can be rationalized using the Goldschmidt tolerance factor, *t*, which quantifies the relationship between the stability of the perovskite structure and the radii of the ions [22]. Tolerance factors, calculated using Structure Prediction Diagnostic Software (SPuDS) [23], begin with the previously reported, La_2MgIrO_6 (t=0.9217) [2,9], and continue to decrease in value to Gd_2MgIrO_6 (t=0.8850). Tb_2MgIrO_6 (t=0.8737) is only slightly smaller than the calculated value for Gd_2MgIrO_6, but appears to fall just below the limiting value of t=0.8850 for this series (see Table 3). On the basis of ionic radii, one could postulate that the *B*-site substitution with a smaller divalent cation like Ni^{2+} (CN-6=0.69 Å), for example, may result in the stabilization of analogs containing the smaller lanthanide elements and larger *t* values as calculated for Tb_2NiIrO_6 (t=0.8820).

3.3. Magnetic properties

3.3.1. Pr_2MgIrO_6

The temperature dependence of the susceptibility for Pr_2MgIrO_6 in an applied field of 10 kG is shown in Fig. 3. Fitting the high-temperature susceptibility ($100\,K < T < 300\,K$) to the Curie–Weiss law results in values of μ_{eff}=5.16 μ_B, C=3.37 emu/mol K, and $\theta = -23$ K. This moment is slightly lower than the theoretical value of 5.35 μ_B. The small negative Weiss temperature (−23 K) is indicative of weak antiferromagnetic interactions, and the plot shows a downturn in the susceptibility corresponding to an antiferromagnetic transition (T_N=14 K).

3.3.2. Nd_2MgIrO_6

The temperature dependence of the susceptibility for Nd_2MgIrO_6 in an applied field of 10 kG is shown in Fig. 4. Fitting the high-temperature susceptibility ($100\,K < T < 300\,K$) to the

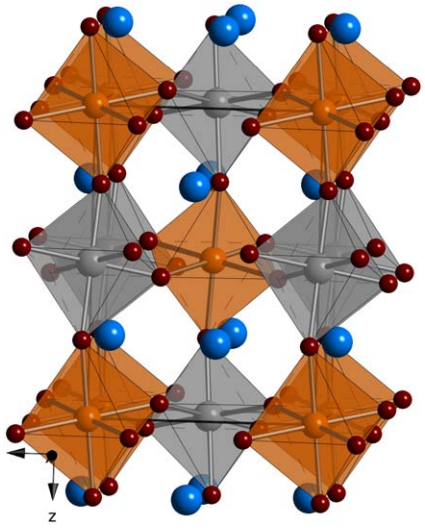

Fig. 2. The crystal structure of Nd_2MgIrO_6 is shown and is representative of the general structure observed in the Ln_2MgIrO_6 (*Ln*=Pr, Nd, Sm, Eu, Gd) double perovskite series. Iridium atoms are gray octahedra, magnesium atoms are orange octahedra, neodymium atoms are blue spheres, and oxygen atoms are red spheres. (For interpretation of the references to color in this figure legend, the reader is referred to the web version of this article.)

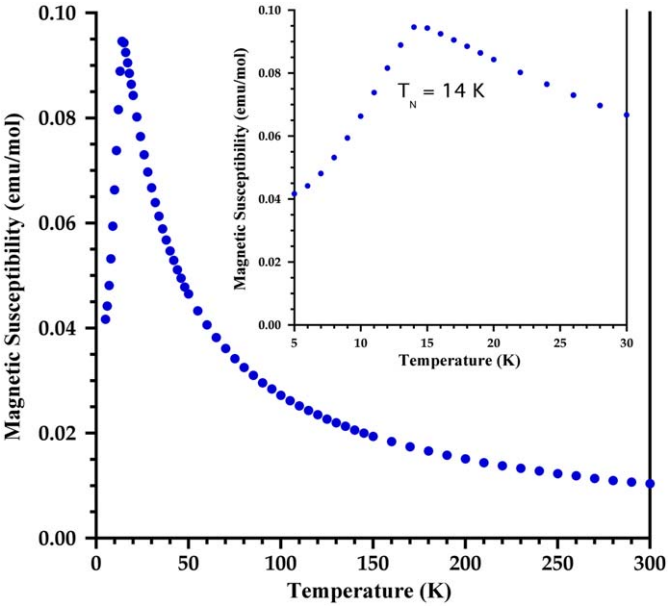

Fig. 3. The temperature dependence of the magnetic susceptibility of Pr_2MgIrO_6 in an applied field of 10 kG.

Curie–Weiss law results in values of μ_{eff}=5.17 μ_B, C=3.33 emu/mol K, and θ=−25 K. This moment agrees well with the theoretical moment (5.40 μ_B). The small, negative Weiss temperature (−25 K) is indicative of weak antiferromagnetic interactions and the downturn in the susceptibility corresponds to an antiferromagnetic interaction (T_N=12 K).

3.3.3. Sm_2MgIrO_6

The temperature dependence of the susceptibility for Sm_2MgIrO_6 in an applied field of 10 kG is shown in Fig. 5. The compound orders antiferromagnetically as indicated by the downturn in the susceptibility plot, which corresponds to an antiferromagnetic transition temperature, T_N, of 15 K.

3.3.4. Eu_2MgIrO_6

The temperature dependence of the susceptibility for Eu_2MgIrO_6 in an applied field of 10 kG is shown in Fig. 6. The compound orders antiferromagnetically as indicated by the downturn in the susceptibility plot, which corresponds to an antiferromagnetic transition temperature, T_N, of 10 K.

3.3.5. Gd_2MgIrO_6

The temperature dependence of the susceptibility for Gd_2MgIrO_6 in an applied field of 10 kG is shown in Fig. 7. Fitting the high-temperature susceptibility (150 K < T < 300 K) to the Curie–Weiss law results in values of μ_{eff}=10.68 μ_B, C=14.42 emu/mol K, and

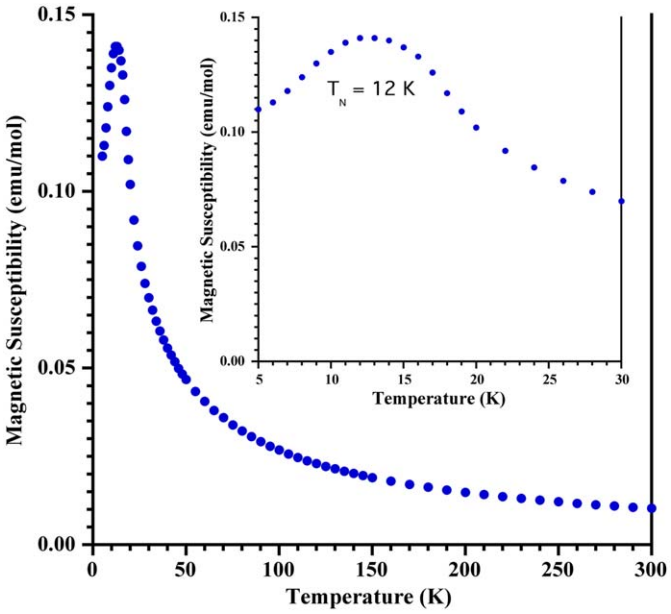

Fig. 4. The temperature dependence of the magnetic susceptibility of Nd_2MgIrO_6 in an applied field of 10 kG.

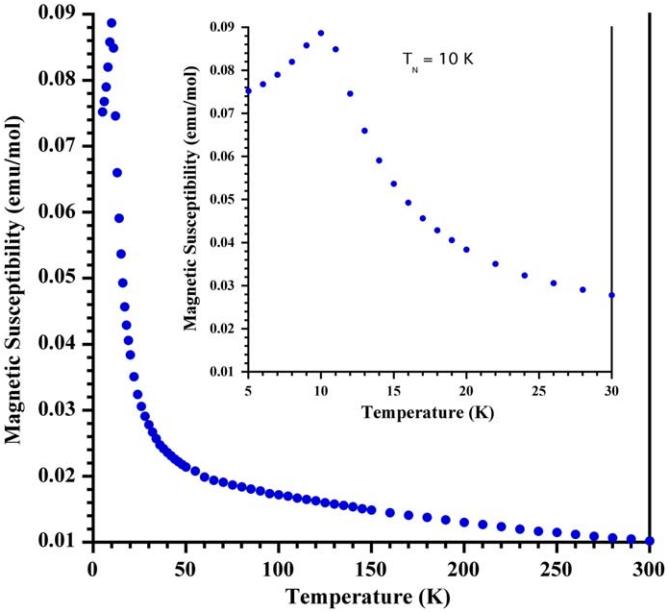

Fig. 6. The temperature dependence of the magnetic susceptibility of Eu_2MgIrO_6 in an applied field of 10 kG.

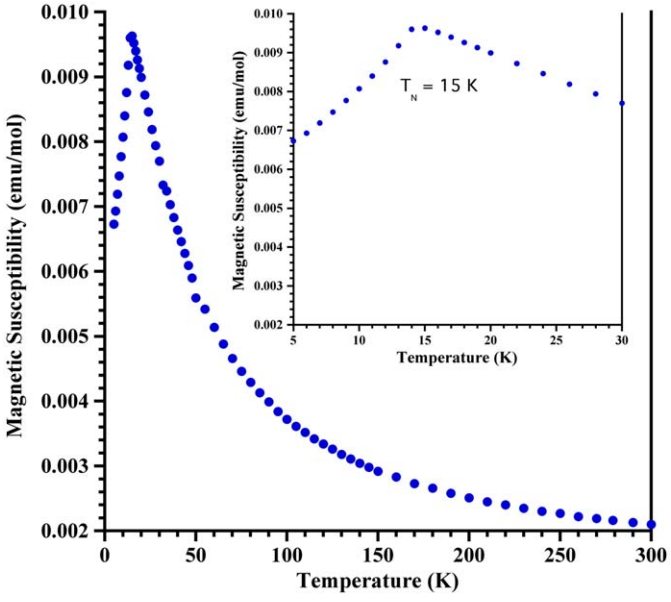

Fig. 5. The temperature dependence of the magnetic susceptibility of Sm_2MgIrO_6 in an applied field of 10 kG.

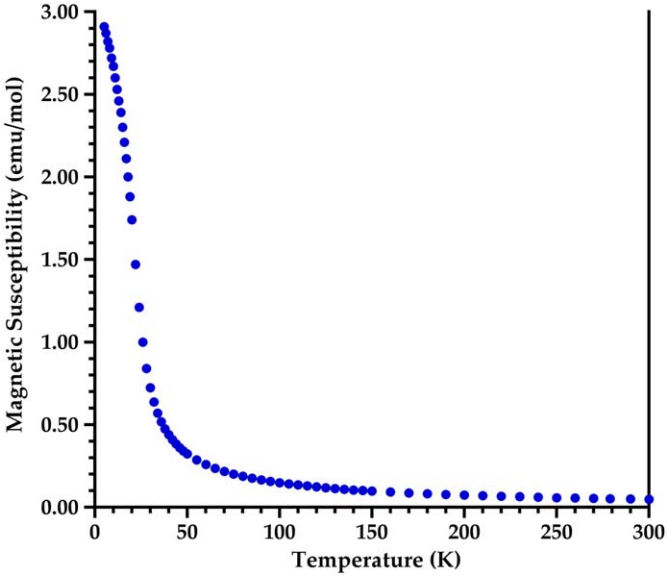

Fig. 7. The temperature dependence of the magnetic susceptibility of Gd_2MgIrO_6 in an applied field of 10 kG.

θ=3 K. This moment is slightly lower than the theoretical moment (11.36 μ_B). Unlike for the other compositions, there is no clear cusp in the magnetic susceptibility plot.

4. Conclusion

Single crystals of a new series of lanthanide-containing monoclinically distorted double perovskites, Ln_2MgIrO_6 (Ln=Pr, Nd, Sm, Eu, Gd) were grown from potassium hydroxide melts. Magnetic susceptibility measurements reveal the presence of antiferromagnetic interactions around 10–15 K in Pr_2MgIrO_6, Nd_2MgIrO_6, Sm_2MgIrO_6, and Eu_2MgIrO_6.

Supplementary information

Further details of the crystal structure investigations can be obtained from the Fachinformationszentrum Karlsruhe, 76344 Eggenstein-Leopoldshafen, Germany (Fax: +49 7247 808 666; e-mail: crystdata@fiz-karlsruhe.de) on quoting the depository numbers CSD-420874-420878.

Acknowledgment

Financial support from the National Science Foundation through Grant DMR: 0804209 is gratefully acknowledged.

References

[1] R.M. Mitchell, Perovskites: Modern and Ancient, Almaz Press, Thunder Bay, 2002.
[2] A.V. Powell, J.G. Gore, P.D. Battle, J. Alloys Compd. 201 (1993) 73.
[3] W.R. Gemmill, M.D. Smith, R. Prozorov, H.-C. zur Loye, Inorg. Chem. 44 (2005) 2639.
[4] W.R. Gemmill, M.D. Smith, H.C. zur Loye, J. Solid State Chem. 179 (2006) 1750.
[5] M.J. Davis, S.J. Mugavero III, K.I. Glab, M.D. Smith, H.-C. zur Loye, Solid State Sci. 5 (2004) 413.
[6] W.R. Gemmill, M.D. Smith, H.-C. zur Loye, J. Solid State Chem. 177 (2004) 3560.
[7] S.J. Mugavero III, I.V. Puzdrjakova, M.D. Smith, H.-C. zur Loye, Acta Crystallogr. E 61 (2005) i3.
[8] D.M. Giaquinta, H.-C. zur Loye, Chem. Mater. 6 (1994) 365.
[9] R.C. Currie, J.F. Vente, E. Frikkee, D.J.W. IJdo, J. Solid State Chem. 116 (1995) 199.
[10] H. Nishimine, M. Wakeshima, Y. Hinatsu, J. Solid State Chem. 177 (2004) 739.
[11] S.J. Mugavero III, W.R. Gemmill, I.P. Roof, H.C. zur Loye, J. Solid State Chem. 182 (2009) 1950.
[12] S.J. Mugavero III, M.D. Smith, W.-S. Yoon, H.C. zur Loye, Angew. Chem. Int. Ed. 48 (2009) 215.
[13] S.J. Mugavero III, M.D. Smith, H.C. zur Loye, Solid State Sci. 9 (2007) 555.
[14] SMART Version 5.630, SAINT+ Version 6.45, SADABS Version 2.10, Bruker Analytical X-ray Systems, Inc., Madison, 2003.
[15] S.J. Mugavero III, M.D. Smith, H.-C. zur Loye, J. Solid State Chem. 178 (2005) 200.
[16] R.D. Shannon, Acta Crystallogr. A 32 (1976) 751.
[17] S.J. Mugavero III, M.D. Smith, H.-C. zur Loye, J. Solid State Chem. 178 (2005) 3176.
[18] S.J. Mugavero III, M.D. Smith, H.C. zur Loye, Inorg. Chem. 45 (2006) 946.
[19] P.M. Woodward, Acta Crystallogr. B 53 (1997) 44.
[20] P.M. Woodward, Acta Crystallogr. B 53 (1997) 32.
[21] A.M. Glazer, Acta Crystallogr. B 28 (1972) 3384.
[22] V.M. Goldschmidt, Mat.-Nat. Kl. 2 (1926) 117.
[23] M.W. Lufaso, P.M. Woodward, Acta Crystallogr. B 57 (2001) 725.